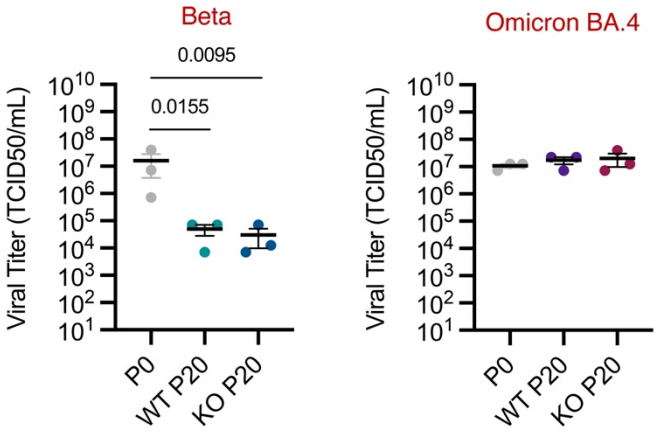

Supplementary Figure 1. Passaged virus in primary HBE cell cultures. Viral titers from SARS-CoV-2 infection of primary HBE cell cultures (error bars represent SEM, p-values by one-way ANOVA with multiple comparisons, n = 3 per group). Source data are provided as a Source Data file.

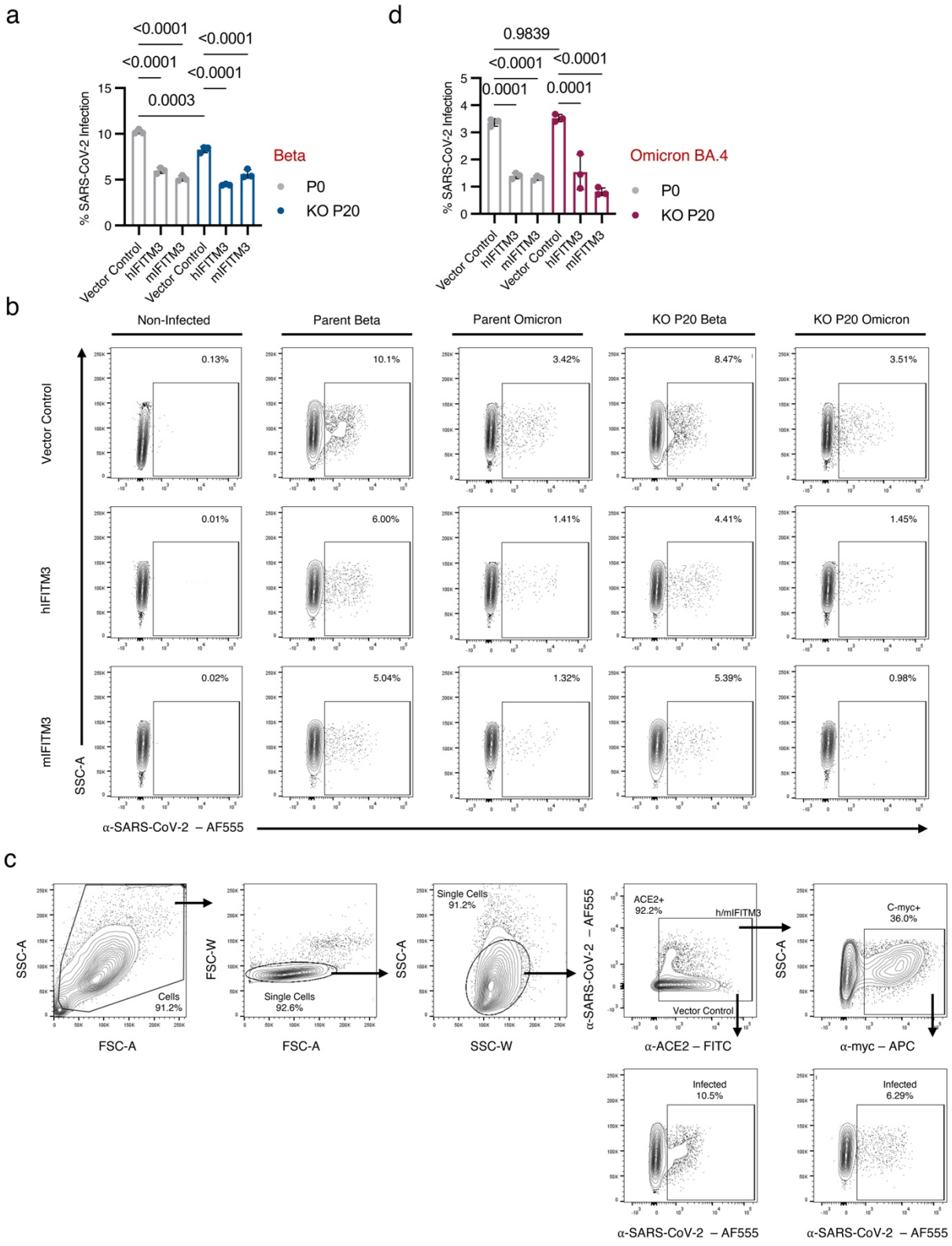

Supplementary Figure 2. Passaged virus in ACE2-HEK293T cell cultures. (**a-b**) Viral titers from SARS-CoV-2 infection of ACE2-HEK293T cell cultures (error bars represent SEM, p-values

represent one-way ANOVA with multiple comparisons, n = 3 per group). (**c**) Representative flow plots for **a-b**. (**d**) Representative gating strategy for (**a-b**). Source data are provided as a Source Data file.

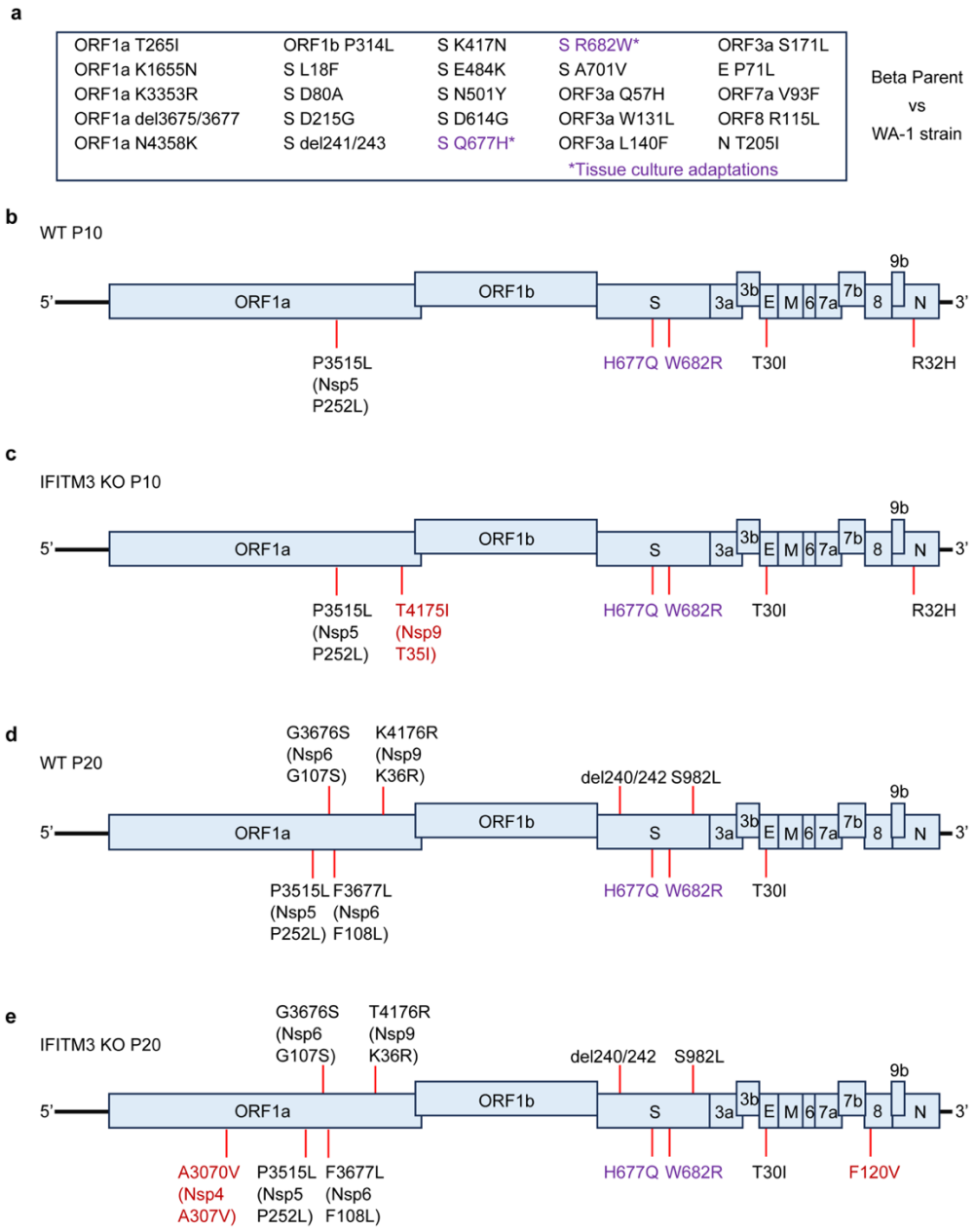

Supplementary Figure 3. Mutations observed within the SARS-CoV-2 beta strain genome after passaging through WT or *Ifitm3*$^{-/-}$ mice. (**a**) List of amino acid differences between the SARS-CoV-2 Beta parent stock and the original WA1 strain. Tissue culture adaptations are indicated with an asterisk (*) and are colored purple. (**b, c**) Schematic of SARS-CoV-2 Beta strain genome annotated with amino acid substitutions found in the consensus sequence after

passaging 10 times (**b**) or 20 times (**c**) through WT mice. (**d, e**) Schematic of SARS-CoV-2 Beta strain genome annotated with amino acid substitutions found in the consensus sequence after passaging 10 times (**d**) or 20 times (**e**) through *Ifitm3*$^{-/-}$ mice.

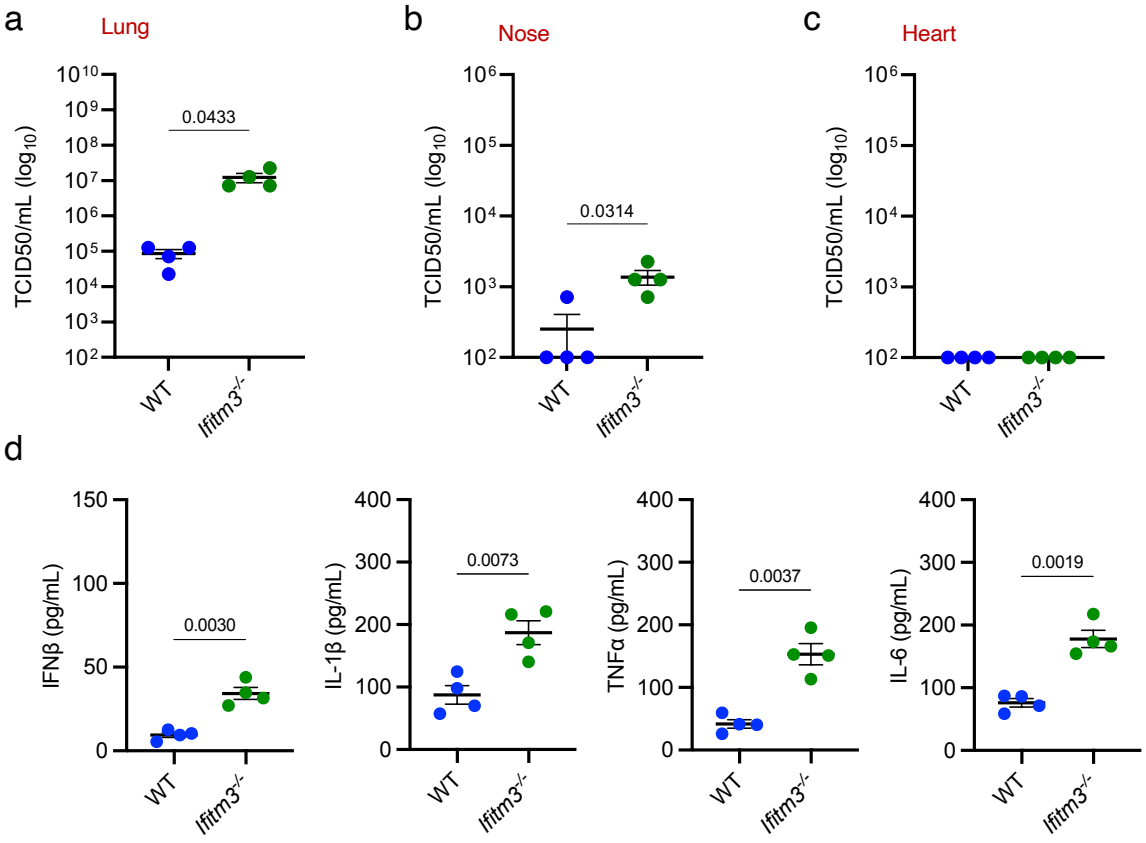

Supplementary Figure 4. IFITM3 restricts the BA.4 omicron virus in mice. Groups of WT or *Ifitm3*$^{-/-}$ mice (n=4 per group) were challenged with 10^5 TCID50 of the SARS-CoV-2 BA.4 strain. Viral titers from lung (**a**) or nose (**b**) homogenates collected at day 2 post infection. (**c**) ELISA quantification of IFNβ, IL-1β, TNFα, and IL-6 in lung homogenates collected at day 2 post infection. Each dot represents an individual mouse. Numbers above the graph represent p values. Source data are provided as a Source Data file.

a

ORF1a S135R	ORF1b P314L	S G339D	S N440K	S Y505H	S Q954H	N P13L
ORF1a del141/143	ORF1b R1315C	S S371F	S L452R	S D614G	S N969K	N R203K
ORF1a T842I	ORF1b I1566V	S S373P	S S477N	S H655Y	ORF3a T223I	N G204R
ORF1a G1307S	ORF1b T2163I	S S375F	S T478K	S N679K	E T9I	
ORF1a L3027F	S T19I	S T376A	S E484A	S P681H	M D3N	
ORF1a T3090I	S del25/27	S D405N	S F486V	S413R	M Q19E	
ORF1a T3255I	S G142D	S R408S	S Q498R	S N764K	M A63T	
ORF1a P3395H	S V213G	S K417N	S N501Y	S D796Y	ORF6 D61L	

Omicron Parent vs WA-1 strain

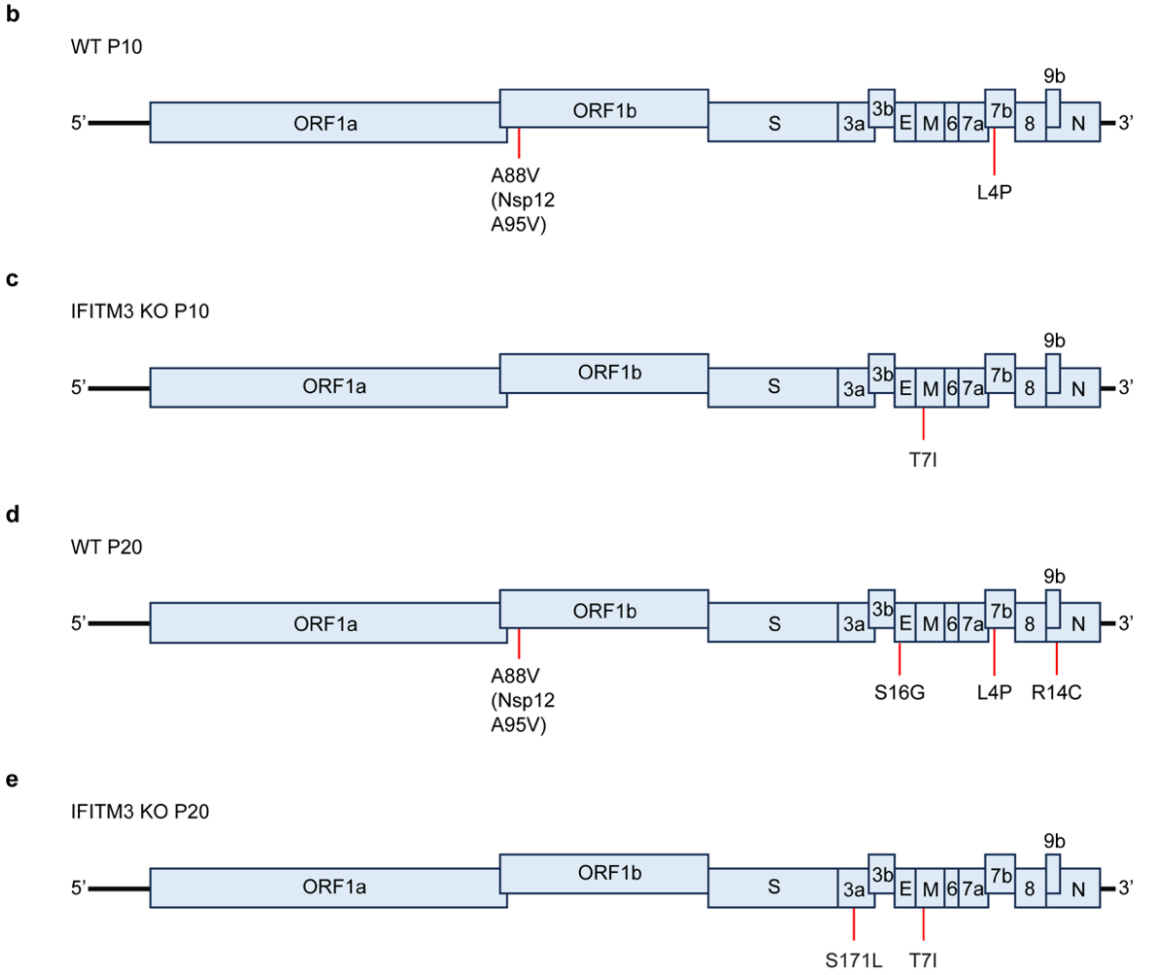

Supplementary Figure 5. Mutations observed within the SARS-CoV-2 BA.4 strain genome after passaging through WT or *Ifitm3*$^{-/-}$ mice. (a) List of amino acid differences between the SARS-CoV-2 Beta parent stock and the original WA1 strain. (**b, c**) Schematic of SARS-CoV-2 BA.4 strain genome annotated with amino acid substitutions found in the consensus sequence after passaging 10 times (**b**) or 20 times (**c**) through WT mice. (**d, e**) Schematic of SARS-CoV-2 BA.4 strain genome annotated with amino acid substitutions found in the consensus sequence after passaging 10 times (**d**) or 20 times (**e**) through *Ifitm3*$^{-/-}$ mice.

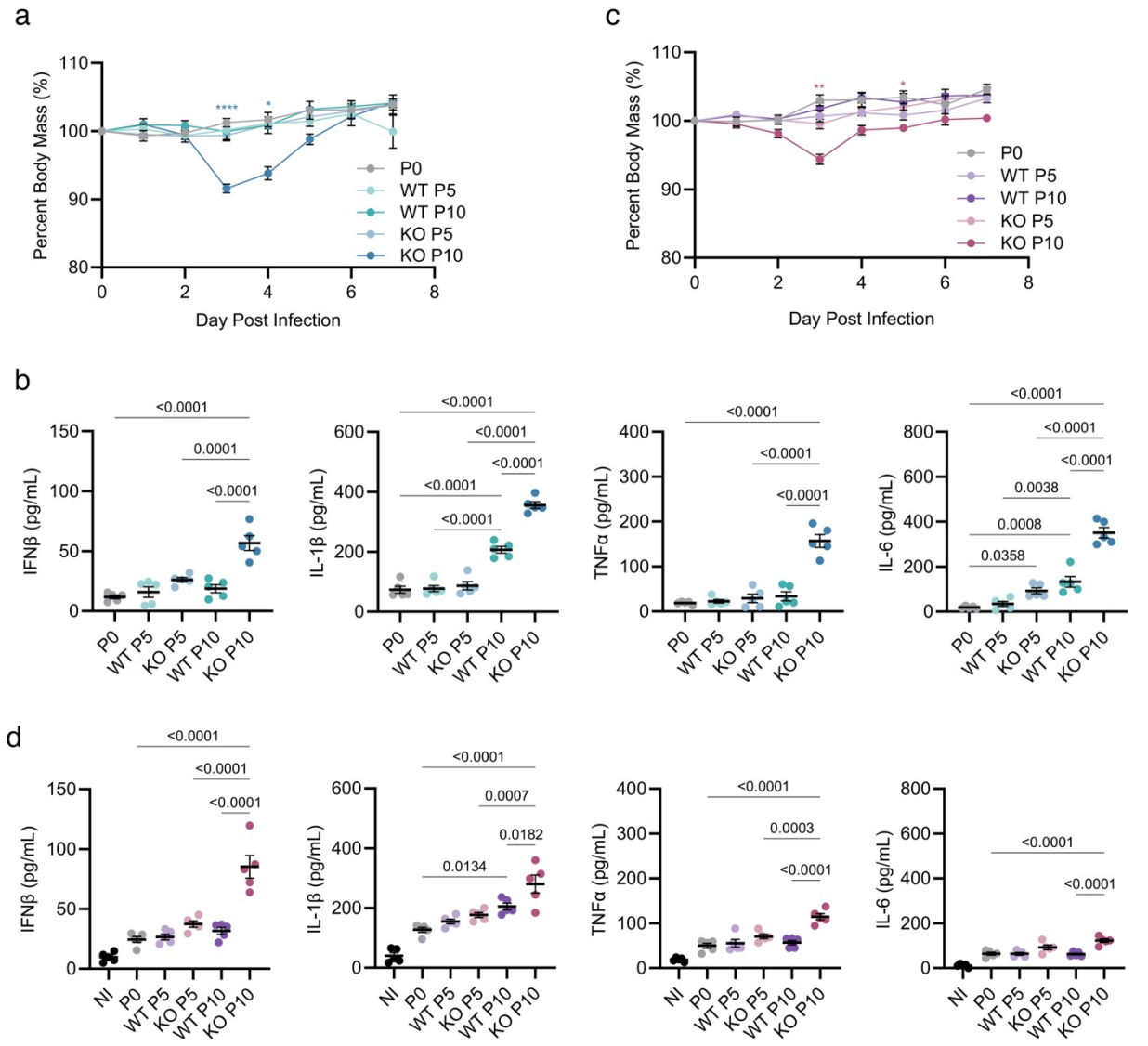

Supplementary Figure 6. Passaging SARS-CoV-2 variants 10 times through *Ifitm3*$^{-/-}$ mice is sufficient to induce greater weight loss and inflammatory cytokines. Groups of WT mice (n=5 per group) were challenged with 10^5 TCID50 of the SARS-CoV-2 Beta (**a, b**) or Omicron BA.4 (**c, d**) strains passaged 5 or 10 times through WT or *Ifitm3*$^{-/-}$ mice and compared to the parent virus (passage 0). (**a, c**) Weight loss during challenge by passaged SARS-CoV-2 viruses. Error bars represent SEM, comparisons were made using the Mann-Whitney test (only comparisons between P0, WT P10, and KO P10 are shown (p values: *** <0.0005, ** <0.005, *<0.05). Dots represent averages of individual mice (n=5 per group). (**b, d**) ELISA quantification of IFNβ, IL-1β, TNFα, and IL-6 in lung homogenates collected at day 2 post infection. Each dot represents an individual mouse. Numbers above the graph represent p values. Source data are provided as a Source Data file.

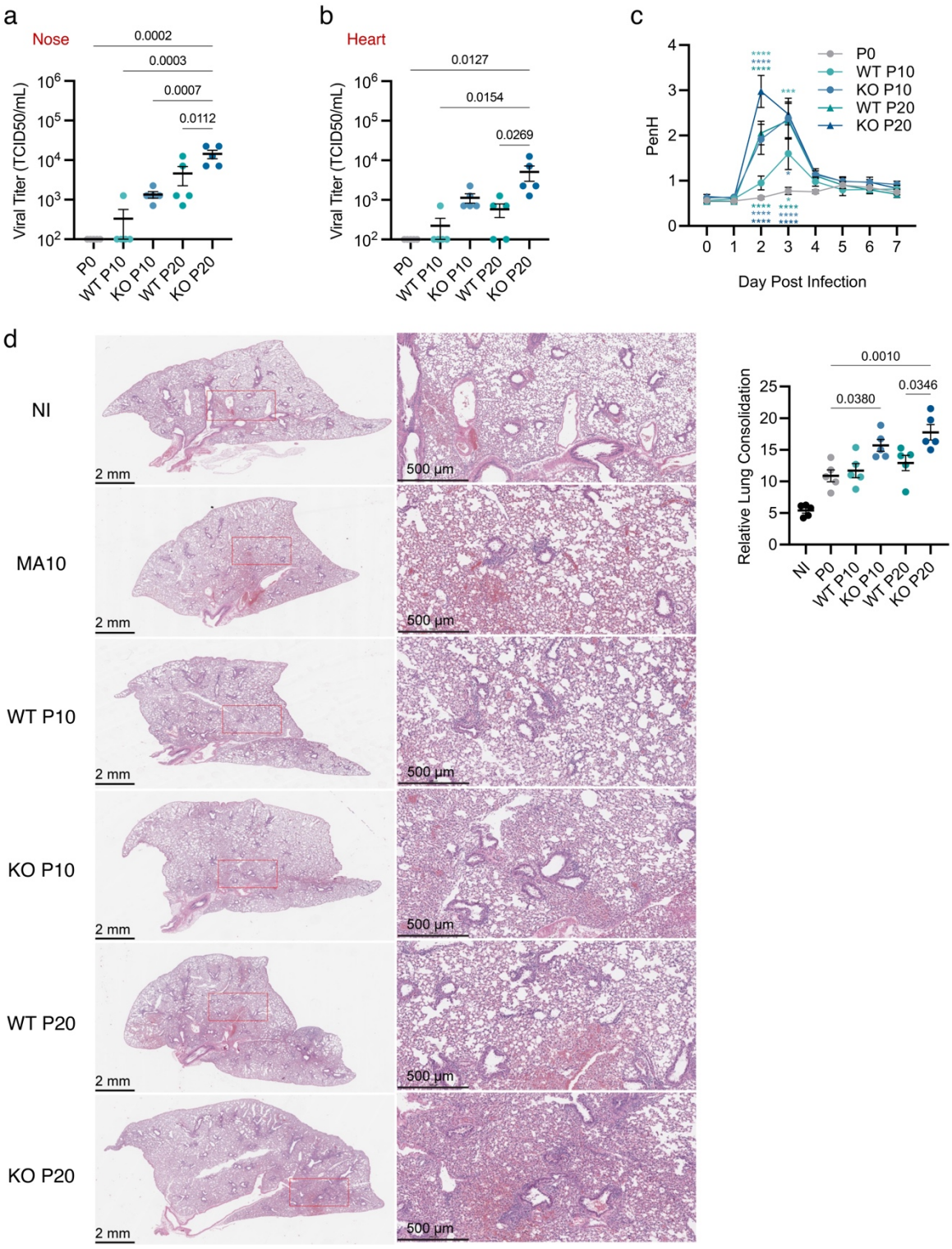

Supplementary Figure 7. Comparing lung pathogenesis and inflammation induced by the SARS-CoV-2 Beta strain passaged 10 or 20 times through WT or *Ifitm3*$^{-/-}$ mice. Groups of WT mice (n=5 per group) were challenged with 10^5 TCID50 of the SARS-CoV-2 Beta strain passaged 10 or 20 times through WT or *Ifitm3*$^{-/-}$ mice and compared to the parent virus (passage

0). Viral titers from nose (**a**), or heart (**b**) homogenates collected at day 2 post infection. (**c**) Daily whole-body plethysmography enhanced pause (PenH) measurements. Dots represent averages of individual mice (n=5 per group) (p values: **** <0.0001, *** <0.0005, ** <0.005, *<0.05). (**d**) Representative histology images of infected lungs at day 7 post infection. Whole lung images are shown on the left (scale bars represent 2 mm) and 4x zoomed images are shown on the right (scale bars represent 500 μm). The red box present in the whole lung images corresponds to its matched zoomed in image. (**e**) Quantification of consolidated tissue versus open airspace in H&E staining for entire lung sections of multiple animals infected at day 7 post infection. (**a, b, e**) Each dot represents an individual mouse. (**c**) Dots represent averages of individual mice (n=5 per group). Source data are provided as a Source Data file.

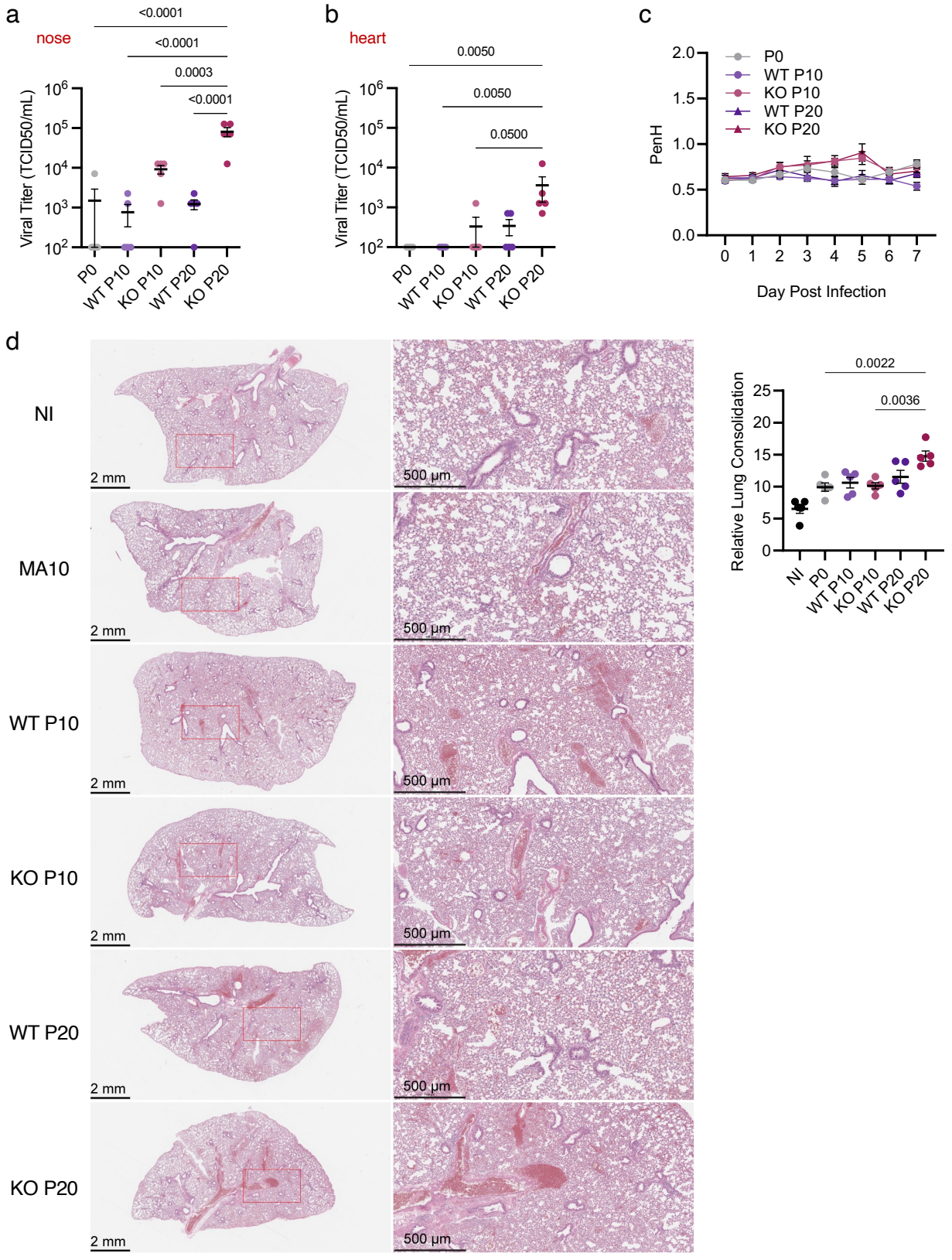
a
nose
<0.0001
<0.0001
0.0003
<0.0001
Viral Titer (TCID50/mL)
P0
WT P10
KO P10
WT P20
KO P20
b
heart
0.0050
0.0050
0.0500
c
PenH
Day Post Infection
d
NI
MA10
WT P10
KO P10
WT P20
KO P20
2 mm
500 µm
Relative Lung Consolidation
0.0022
0.0036

Supplementary Figure 8. Comparing lung pathogenesis and inflammation induced by the SARS-CoV-2 Omicron BA.4 strain passaged 10 or 20 times through WT or *Ifitm3*$^{-/-}$ mice. Groups of WT mice (n=5 per group) were challenged with 10^5 TCID50 of the SARS-CoV-2 BA.4 strain passaged 10 or 20 times through WT or *Ifitm3*$^{-/-}$ mice and compared to the parent virus (passage 0). Viral titers from nose (**a**), or heart (**b**) homogenates collected at day 2 post infection. (**c**) Daily whole-body plethysmography enhanced pause (PenH) measurements. Dots represent averages of individual mice (n=5 per group). (**d**) Representative histology images of infected lungs at day 7 post infection. Whole lung images are shown on the left (scale bars represent 2 mm) and 4x zoomed images are shown on the right (scale bars represent 500 μm). The red box present in the whole lung images corresponds to its matched zoomed in image. (**e**) Quantification of consolidated tissue versus open airspace in H&E staining for entire lung sections of multiple animals infected at day 7 post infection. (**a, b, e**) Each dot represents an individual mouse. (**c**) Dots represent averages of individual mice (n=5 per group). Source data are provided as a Source Data file.

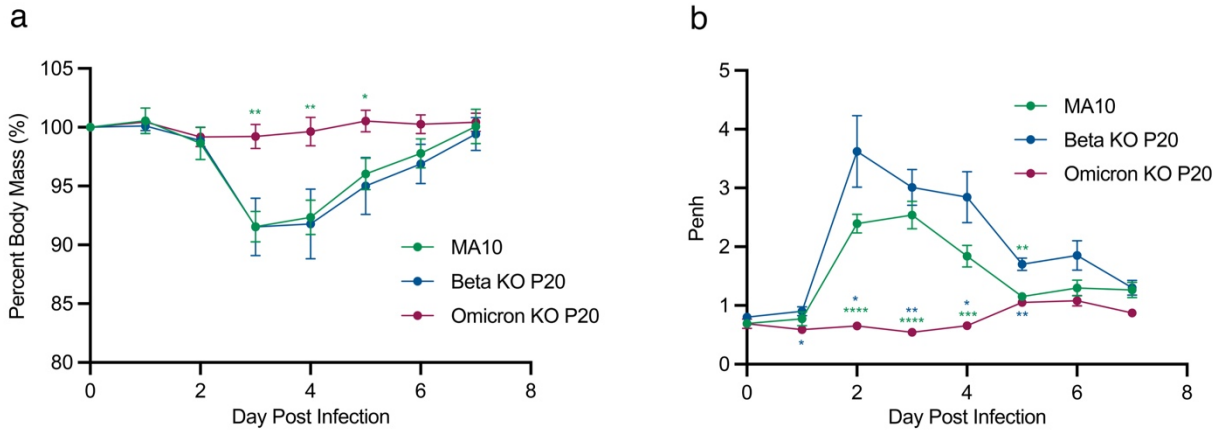

Supplementary Figure 9. Comparative analysis of mouse-adapted Beta, Omicron, and MA10 strains in WT Balb/c mice. Groups of WT mice (WT n=5, Beta KO P20 n=5, Omicron KO P20 n=5) were challenged with 10^5 TCID50 of the SARS-CoV-2 BA.4 strain or Beta strain passaged 20 times through *Ifitm3*$^{-/-}$ mice and compared to infection by an equal dose of MA10. (**a**) Weight loss during challenge by passaged SARS-CoV-2 viruses. (**b**) Daily whole-body plethysmography enhanced pause (PenH) measurements. (**a, b**) Dots represent averages of individual mice. Error bars represent SEM, comparisons were made using a two-way ANOVA with Tukey's multiple comparisons. (p values: **** <0.0001, *** <0.0005, ** <0.005, *<0.05, exact p values are provided in Source Data). Source data are provided as a Source Data file.

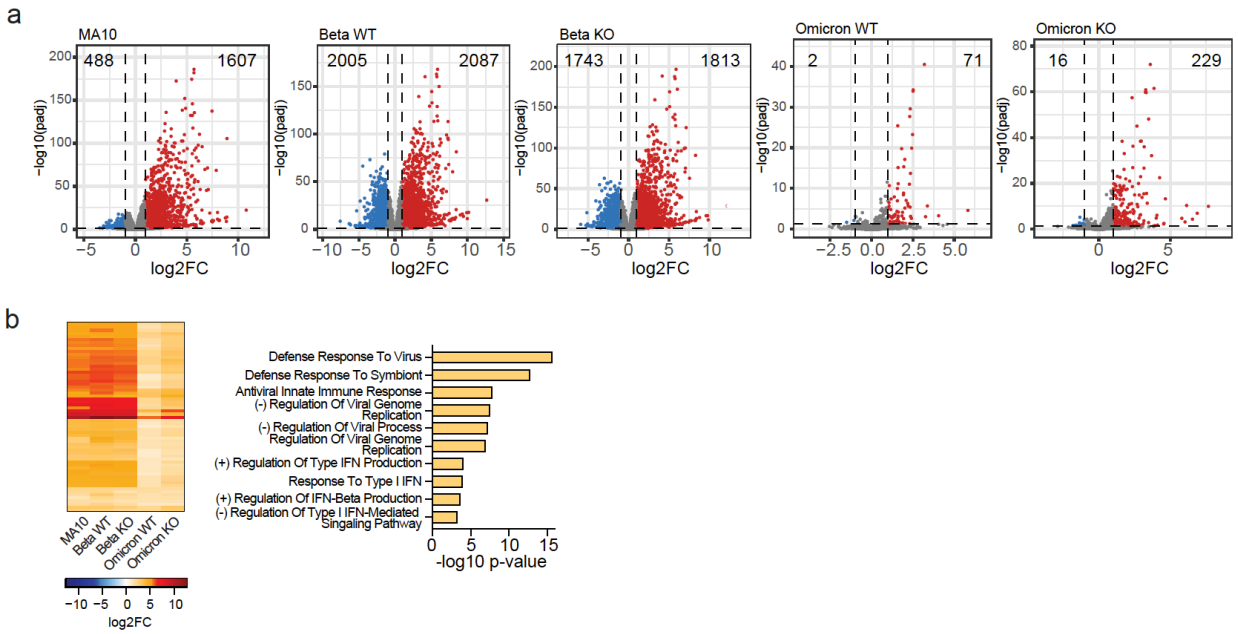

Supplementary Figure 10. SARS-CoV-2 variants elicit innate immune activation in the lungs of infected mice. (**a**) Volcano plots depict the magnitude (x axis) and significance (y axis) of change in gene expression at day two post-infection. Each data point represents a unique transcript, where color denotes upregulation (red) or downregulation (blue) in expression relative to mock-inoculated mice. Dashed lines depict significance cutoffs (lfc |1|, padj <0.05) and grey data points depict non-significant genes. The number of DEG in either is highlighted in the top corners of the graphs. (**b**) Euclidean distance-based hierarchical clustering of the 63 DEG that overlap across all infectious conditions. Color indicates upregulation (red) in gene expression (left). Bar graphs represent the enrichment scores of GO Biological Pathways terms identified by EnrichR. Each node represents a unique term, edges represent connectivity across terms. Color indicates significant enrichment across infectious groups as indicated by the color scale.

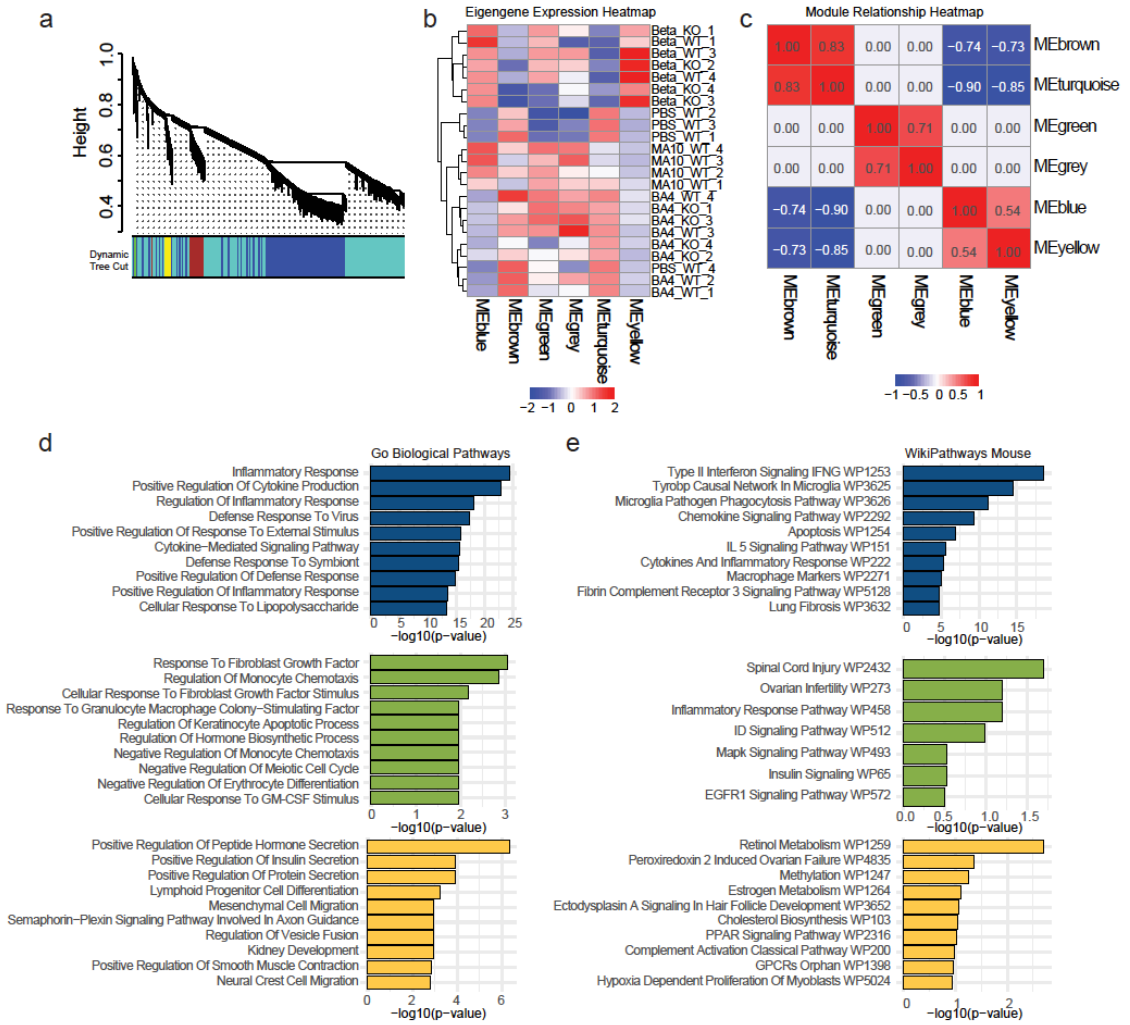

Supplementary Figure 11. Network analysis reveals gene expression modules associated with viral disease. (**a**) Hierarchical clustering dendrogram of genes with module assignments based on co-expression patterns. Modules were defined using the dynamic tree cut algorithm, and unassigned genes were assigned to the 'grey' module. Modules were distinguished by unique colors shown below the dendrogram. (**b**) Heatmap of scaled (Z-score transformation) module eigengene (ME) expression levels with rows representing individual samples, and columns corresponding co-expression network modules. Row-based hierarchical clustering based on their ME expression profiles was performed. The color scale indicates low (blue) to high (red) expression levels. (**c**) Heatmap of significant pairwise Person's correlations between module eigengenes (MEs). Rows and columns represent modules, clustered based on similarity in their eigengene expression profiles. Non-significant correlations ($p > 0.05$) were set to zero. The color scale indicates positive (red), negative (blue), or no correlations (white). (**d, e**) Bargraphs represent the -log10 padj significance values of the top d) GO Biological Pathways and e) WikiPathways Mouse terms identified in the 'brown' module using EnrichR.

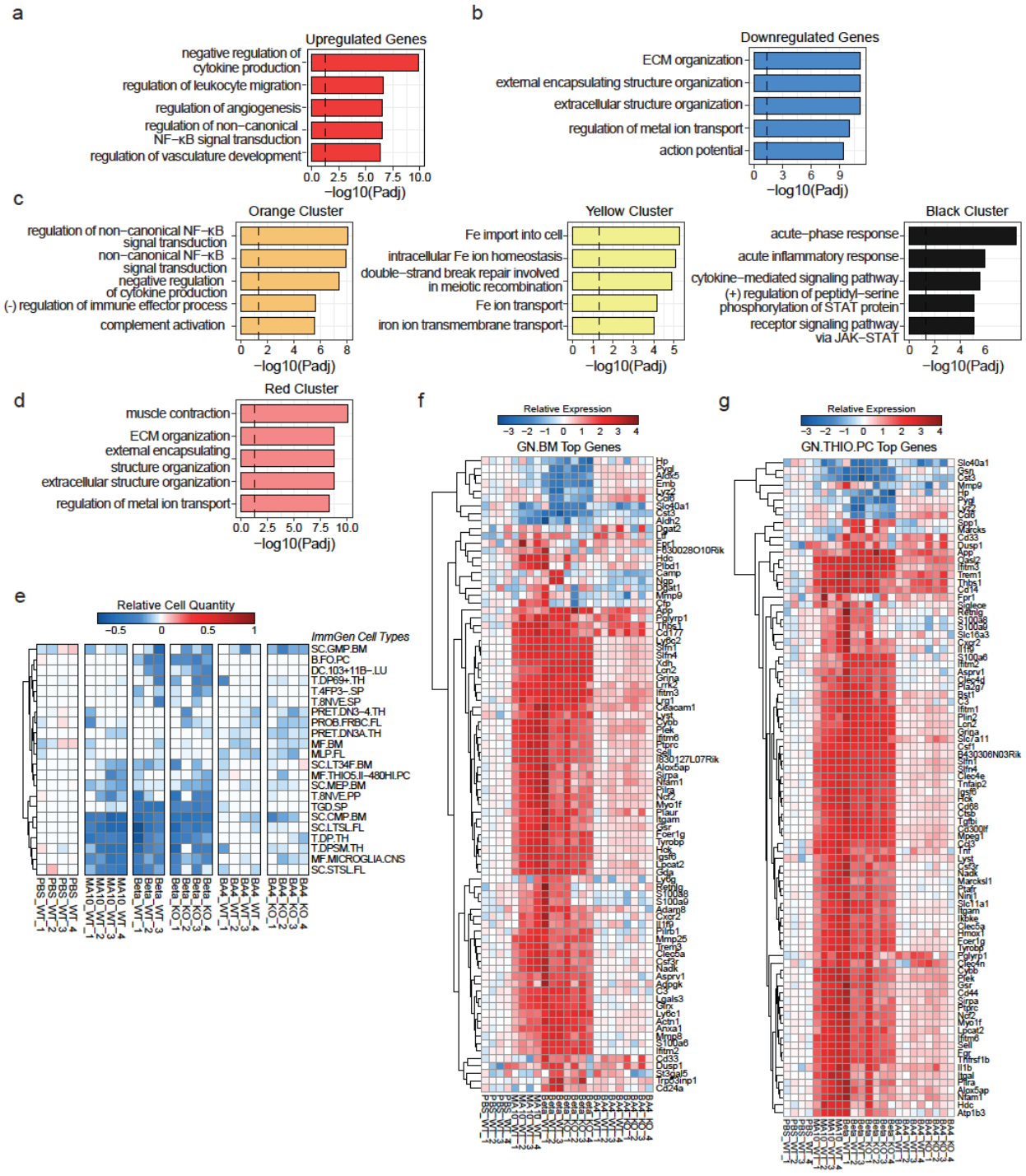

Supplementary Figure 12. Turquoise model reveals changes in inflammatory responses and extracellular matrix remodeling. Functional enrichment analysis of genes within the Turquiose module. (**a-d**) Bar graphs representing the gene ontology analysis of genes corresponding to (**a**) upregulated, (**b**) downregulated, (**c**) orange, yellow and black, and (**d**) red gene clusters within the Turquoise module identified by hierarchical clustering in Figure 3A. The

x-axis denoted the -log10 padj value of enrichment of the top 10 GO Biological Pathways for each cluster as indicated by color. (**e**) Negatively enriched ImmGen cell types as inferred by DCQ (same as **Figure 7f**). (**f-g**) Heatmap representing expression, relative to PBS control mice, of the top genes contributing to the (**f**) GN.BM and (**g**) GN.THIO.PC ImmGen cell types in the DCQ algorithm. Red indicates greater expression, and blue indicates lower expression, compared to PBS-inoculated control mice.

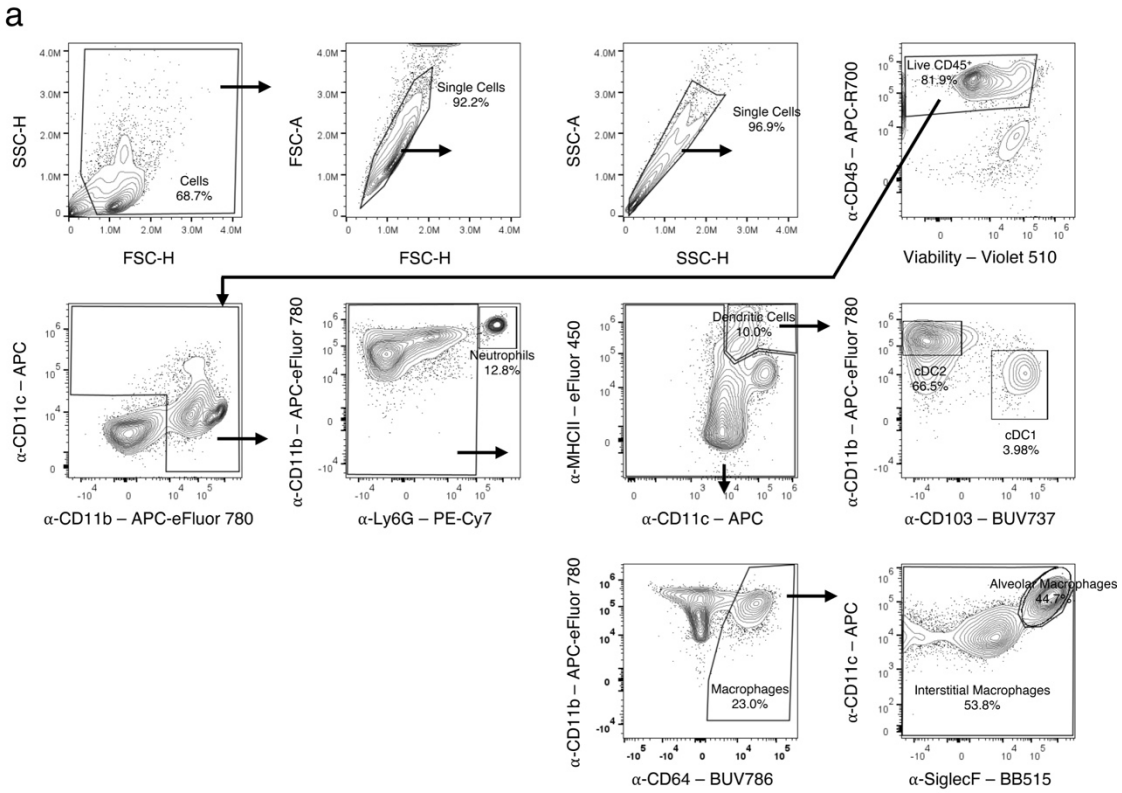
a
SSC-H
FSC-H
Cells
68.7%
FSC-A
FSC-H
Single Cells
92.2%
SSC-A
SSC-H
Single Cells
96.9%
α-CD45 – APC-R700
Viability – Violet 510
Live CD45+
81.9%
α-CD11c – APC
α-CD11b – APC-eFluor 780
α-CD11b – APC-eFluor 780
α-Ly6G – PE-Cy7
Neutrophils
12.8%
α-MHCII – eFluor 450
α-CD11c – APC
Dendritic Cells
10.0%
α-CD11b – APC-eFluor 780
α-CD103 – BUV737
cDC2
66.5%
cDC1
3.98%
α-CD11b – APC-eFluor 780
α-CD64 – BUV786
Macrophages
23.0%
α-CD11c – APC
α-SiglecF – BB515
Alveolar Macrophages
44.7%
Interstitial Macrophages
53.8%

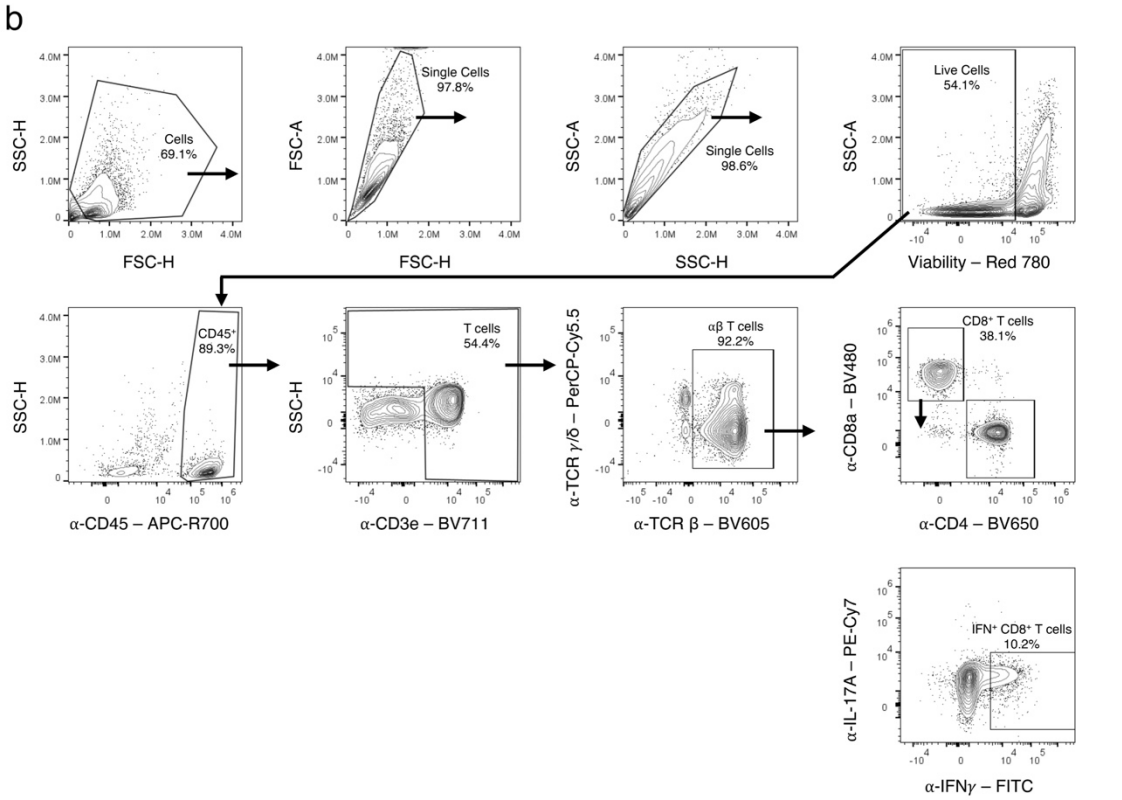
b
SSC-H
FSC-H
Cells
69.1%
FSC-A
FSC-H
Single Cells
97.8%
SSC-A
SSC-H
Single Cells
98.6%
SSC-A
Viability – Red 780
Live Cells
54.1%
SSC-H
α-CD45 – APC-R700
CD45+
89.3%
SSC-H
α-CD3e – BV711
T cells
54.4%
α-TCR γ/δ – PerCP-Cy5.5
α-TCR β – BV605
αβ T cells
92.2%
α-CD8a – BV480
α-CD4 – BV650
CD8+ T cells
38.1%
α-IL-17A – PE-Cy7
α-IFNγ – FITC
IFN+ CD8+ T cells
10.2%

Supplementary Figure 13. Flow cytometry lung immunophenotyping gating strategy. (a) Gating strategy for data generated in Supplementary Fig 14a, b, c, d, and h. (b) Gating strategy for data generated in Supplementary Fig 14e, f, and g.

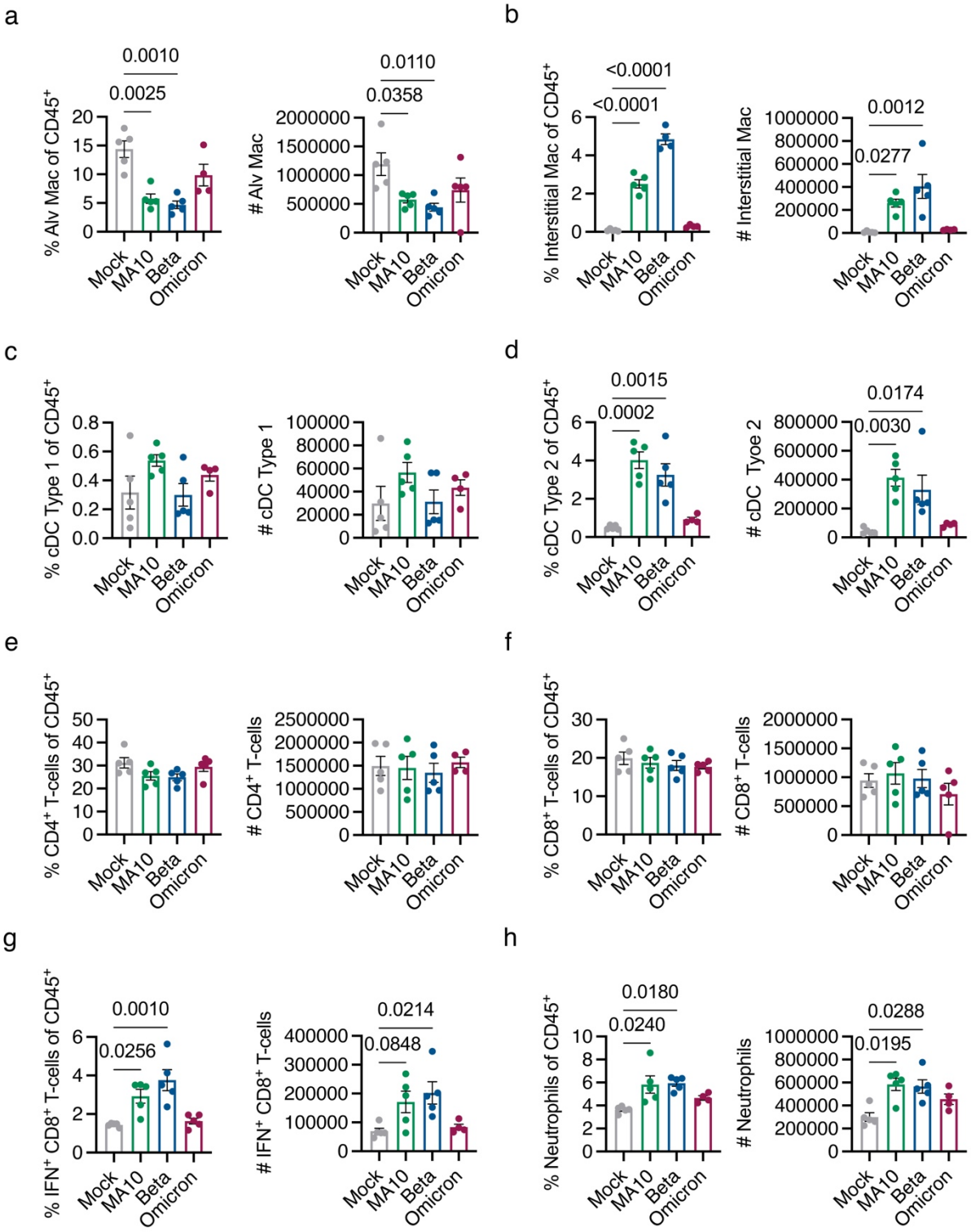

Supplementary Figure 14. Lung immunophenotyping. (**a-h**) Groups of WT mice (n=5 Mock, MA10; n=4 Beta, Omicron) were challenged with 10^5 TCID50 of the indicated mouse adapted SARS-CoV-2 strain. On day 4 post infection, lungs were harvested for immunophenotyping via flow cytometry. Data is presented as % CD45+ (left) or total number (right) for alveolar macrophages (**a**), interstitial macrophages (**b**), conventional dendritic cells type 1 (**c**), conventional dendritic cells type 2 (**d**), CD4+ T cells (**e**), CD8+ T cells (**f**), IFN+ CD8+ T cells (**g**), and neutrophils (**h**) (error bars represent SEM, p-values by one-way ANOVA with multiple comparisons test). Source data are provided as a Source Data file.

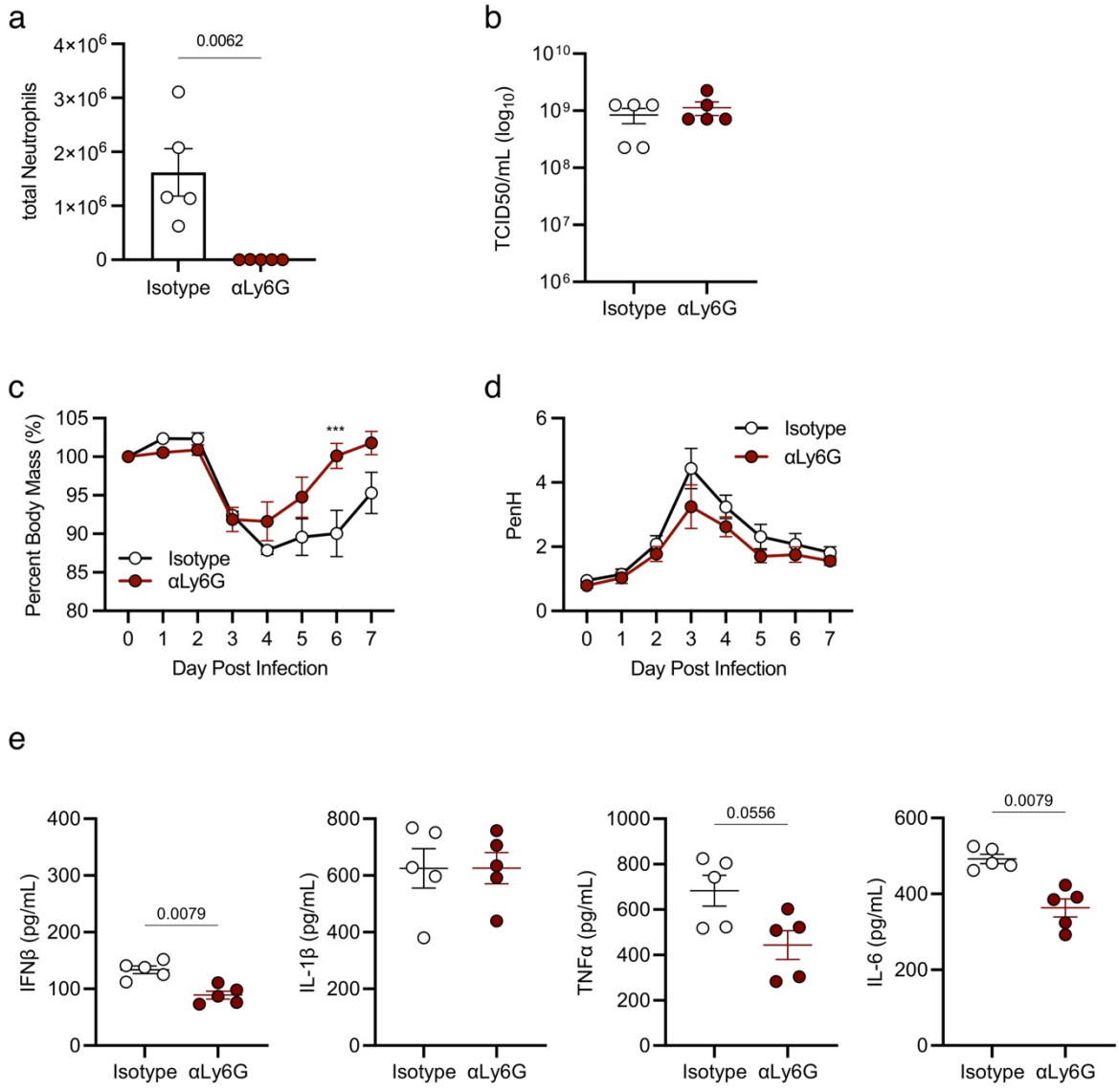

Supplementary Figure 15. Neutrophil depletion reduces disease severity in mice infected with SARS-CoV-2. Groups of WT mice (n=5 per group) were challenged with 10^5 TCID50 of the SARS-CoV-2 Beta strain passaged 20 times through *Ifitm3*$^{-/-}$ mice. To deplete neutrophils, mice were treated with antibodies targeting neutrophils (αLy6G) or an isotype control antibody, starting at day 1 post infection through day 6 post infection. (**a**) Neutrophil number in the lungs of infected mice on day 4 post infection by flow cytometry; error bars indicate SEM, p value above the bar determined by two-tailed unpaired t-test. (**b**) Viral titers from lung homogenates collected at day 2 post infection. (**c**) Weight loss during challenge by passaged SARS-CoV-2 viruses. Error bars represent SEM. Comparisons made by two-way ANOVA followed by Sidak multiple comparisons, exact p-value provided in source data. (**d**) Daily whole-body plethysmography enhanced pause (PenH) measurements. (**e**) ELISA quantification of IFNβ, IL-1β, TNFα, and IL-6 in lung homogenates collected at day 2 post infection. (**a, b, e**) Dots represent individual mice (n=5). (**c, d**) Dots represent averages of individual mice (n=5 per group). Source data are provided as a Source Data file.

Supplementary Table 1. Mouse-adaptive SARS-CoV-2 mutations from the current study and published works.

Protein	
S	**Citations**
N30T	Willet et al. Commun. Biol. 2024
ins 215KLRS	Rathnasinghe et al. Nat. Commun. 2022
del 240/242	Current work
T250A	Beer et al. J. Exp. Med. 2022
S371F	Willet et al. Commun. Biol. 2024
K417N	Sun et al. Nat. Commun. 2021, Beer et al. J. Exp. Med. 2022, & Muruato et al. PLoS Biol. 2021
K417T	Gawish et al. Elife 2022
K417M	Wong et al. Nature 2022
E484K	Wong et al. Nature 2022
Q493H	Sun et al. Nat. Commun. 2021
Q493K	Huang et al. EBioMedicine 2021, Leist et al. Cell 2020, Bader et al. PNAS 2023, & Ueki et al. Viruses 2024
Q493R	Gawish et al. eLife 2022 & Wong et al. Nature 2022
Q498H	Huang et al. EBioMedicine 2021, Beer et al. J. Exp. Med. 2022, Zhang et al. Cell Discov. 2021 & Gawish et al. Elife 2022
Q498R	Wong et al. Nature 2022
N501Y	Gu et al. Science 2020 & Rathnasinghe et al. Nat. Commun. 2022
H655Y	Muruato et al. PLos Biol. 2021, Zhang et al. Cell Discov. 2021, & Rathnasinghe et al. Nat. Commun. 2022
H677Q*	Current work
Q677H	Willet et al. Commun. Biol. 2024
R682W	Willet et al. Commun. Biol. 2024
W682R*	Current work
A684V	Willet et al. Commun. Biol. 2024
A892V	Willet et al. Commun. Biol. 2024
S982L	Current work
E1182G	Willet et al. Commun. Biol. 2024

Mutation in current study

Identical mutation in multiple studies

Residue mutated in multiple studies, with different resulting amino acid changes

*Reversion of known tissue-culture adaptations

N	
R14C	Current work
T16M	Willet et al. Commun. Biol. 2024
R32H	Current work & Willet et al. Commun. Biol. 2024
R32C	Sun et al. Nat. Commun. 2021
D128Y	Gu et al. Science 2020 & Muruato et al. PLoS Biol. 2021
S194T	Rathnasinghe et al. Nat. Commun. 2022
E	
E8V	Muruato et al. PLoS Biol. 2021
S16G	Current work
T30I	Current work
M	
T7I	Current work, Ueki et al. Viruses 2024, Beer et al. J. Exp. Med. 2022, & Rathnasinghe, et al. Nat. Commun. 2022
H125Y	Bader et al. PNAS 2023
Nsp2	
I42V	Willet et al. Commun. Biol. 2024
Nsp3	
P108L	Willet et al. Commun. Biol. 2024
N262T	Zhang et al. Cell Discovery 2021
H682Y	Willet et al. Commun. Biol. 2024
A1197V	Beer et al. J. Exp. Med. 2022
I1258V	Sun et al. Nat. Commun. 2021
Nsp4	
T285I	Leist et al. Cell 2020
T295I	Ueki et al. Viruses 2024, Beer et al. J. Exp. Med 2022, & Wong et al. Nature 2022
A307V	Current work
H313Y	Bader et al. PNAS 2023
H470Y	Sun et al. Nat. Commun. 2021
Nsp5	
P96L	Willet et al. Commun. Biol. 2024
C160F	Willet et al. Commun. Biol. 2024
P252L	Current work & Willet et al. Commun. Biol. 2024
F294L	Ueki et al. 2024 & Huang et al. EBioMedicine 2021
S301L	Sun et al. Nat. Commun. 2021

Nsp6	
I7T	Huang et al. EBioMedicine 2021
L37F	Gu et al. Science 2020
G107S	Current work
F108L	Current work
A128V	Sun et al. Nat. Commun. 2021
Nsp7	
K2R	Leist et al. Cell 2020
S8F	Sun et al. Nat. Commun. 2021
Nsp8	
Q19R	Bader et al. PNAS 2023 & Zhang et al. Cell Discov. 2021
E23G	Leist et al. Cell 2020
S76F	Wong et al. Nature 2022
E155A	Willet et al. Commun. Biol. 2024
Nsp9	
D25Y	Beer et al. J. Exp. Med 2022
T34A	Beer et al. J. Exp. Med 2022
T35I	Current work
K36R	Current work
R39K	Ueki et al. Viruses 2024
T67A	Wong et al. Nature 2022, Willet et al. Commun. Biol. 2024, & Zhang et al. Cell Discov. 2021
T77I	Huang et al. EBioMedicine 2021
Nsp10	
P84S	Gu et al. Science 2020
P87S	Muruato et al. PLos Biol. 2021
Nsp12	
A95V	Current work
Nsp13	
A362V	Zhang et al. Cell Discov. 2021
P504S	Bader et al. PNAS 2023
Nsp14	
V269I	Zhang et al. Cell Discov. 2021
Orf3a	
S171L	Current work
ORF6	
F7S	Leist et al. Cell 2020
Orf7a	
V82A	Willet et al. Commun. Biol. 2024

T120I	Willet et al. Commun. Biol. 2024
Orf7b	
L4P	Current work
Orf8	
T11I	Willet et al. Commun. Biol. 2024
L84S	Rathnasinghe et al. Nat. Commun. 2022
R115L	Willet et al. Commun. Biol. 2024
F120V	Current work

Supplementary Table 2. Gene Expression Modules.

Module	Gene Counts	Top Hubs	Gene Symbol	kWithin
brown	324	ENSMUSG00000073600	Prob1	143.285862
		ENSMUSG00000032348	Gsta4	139.926939
		ENSMUSG00000022235	Cmbl	138.531859
		ENSMUSG00000063428	Ddo	138.318697
		ENSMUSG00000021236	Entpd5	135.551485
		ENSMUSG00000056174	Col8a2	135.267747
		ENSMUSG00000061322	Dnaic1	134.173733
		ENSMUSG00000034035	Ccdc17	133.822388
		ENSMUSG00000052974	Cyp2f2	133.792858
		ENSMUSG00000064202	4430402I18Rik	133.671696
turquoise	2342	ENSMUSG00000040026	Saa3	1263.10949
		ENSMUSG00000019173	Rab5c	1246.62541
		ENSMUSG00000027984	Hadh	1242.23701
		ENSMUSG00000033429	Mcee	1239.35622
		ENSMUSG00000002658	Gtf2f1	1230.80757
		ENSMUSG00000062980	Cped1	1227.75042
		ENSMUSG00000055172	C1ra	1223.95439
		ENSMUSG00000037820	Tgm2	1223.00324
		ENSMUSG00000040209	Zfp704	1221.33902
		ENSMUSG00000031548	Sfrp1	1219.90224

blue	2049	ENSMUSG00000062593	Lilrb4a	1189.15645
		ENSMUSG00000001131	Timp1	1186.09695
		ENSMUSG00000012519	Mlkl	1182.81876
		ENSMUSG00000024397	Aif1	1180.41394
		ENSMUSG00000045827	Serpinb9	1178.76166
		ENSMUSG00000032322	Pstpip1	1178.69926
		ENSMUSG00000070427	Il18bp	1178.61531
		ENSMUSG00000034947	Tmem106a	1178.58324
		ENSMUSG00000038467	Chmp4b	1175.99989
		ENSMUSG00000027422	Rrbp1	1175.92215
green	44	ENSMUSG00000064348	mt-Tn	8.6627665
		ENSMUSG00000064349	mt-Tc	8.55537484
		ENSMUSG00000090698	Apold1	7.68316216
		ENSMUSG00000064347	mt-Ta	7.67266234
		ENSMUSG00000064340	mt-Tl1	7.3073819
		ENSMUSG00000044786	Zfp36	7.16544473
		ENSMUSG00000064346	mt-Tw	6.90025378
		ENSMUSG00000065420	Mir142b	6.49743833
		ENSMUSG00000048489	8430408G22Rik	6.37595583
		ENSMUSG00000097347	Gm17275	6.37131216
yellow	128	ENSMUSG00000056025	Clca3a1	55.6691522
		ENSMUSG00000031503	Col4a2	53.4985652

		ENSMUSG00000026640	Plxna2	51.199328
		ENSMUSG00000064120	Mocs1	49.7102659
		ENSMUSG00000017707	Serinc3	49.5349561
		ENSMUSG00000024222	Fkbp5	49.2932321
		ENSMUSG00000061878	Sphk1	48.2880207
		ENSMUSG00000033684	Qsox1	47.2360735
		ENSMUSG00000020684	Rasl10b	47.2228742
		ENSMUSG00000022938	Fam3b	45.651529
Unassigned genes (grey)	7	ENSMUSG00000104986	1600023N17Rik	0.15494738
		ENSMUSG00000088054	Mir1968	0.09620483
		ENSMUSG00000085403	Gm13068	0.08505946
		ENSMUSG00000080469	Snord98	0.04296427
		ENSMUSG00000089239	Gm22200	0.0378685
		ENSMUSG00000103768	Gm37856	0.02811522
		ENSMUSG00000087795	Gm25965	0.02461934